
JOURNAL OF THE AMERICAN CHEMICAL SOCIETY

Synthesis of a 10-Oxo-Bilirubin: Effects of the Oxo Group on Conformation, Transhepatic Transport, and Glucuronidation

Qingqi Chen,[†] Michael T. Huggins,[†] David A. Lightner,^{*,†} Wilma Norona,[‡] and Antony F. McDonagh[‡]

Contribution from the Department of Chemistry, University of Nevada, Reno, Nevada 89557-0020, and G.I. Unit and the Liver Center, University of California, San Francisco, California 94143-0538

Received June 1, 1999

Abstract: Bilirubin, the yellow pigment of jaundice, is a linear tetrapyrrole with a methylene group at its center, C(10), a position of crucial importance to its conformation and metabolism. The presence of the central methylene group allows the bilirubin to fold into an intramolecularly hydrogen-bonded conformation. This paper describes the first synthesis of a bilirubin analogue with an oxo group at C(10). The change from CH₂ to C=O, from sp³ to sp², is designed to stress the molecule at its hinge and relax its conformation. Such compounds have been suggested as potential oxidative metabolites of bilirubin in vivo. 10-Oxo-mesobilirubin-XIII α (**1**) is a red crystalline solid, unlike its parent, mesobilirubin-XIII α , which is a bright yellow solid. It is surprisingly polar, relative to the parent, yet it does not exhibit a significantly larger bicarbonate/chloroform partition coefficient. Like the parent, **1** appears to adopt an intramolecularly hydrogen-bonded ridge-tile-like conformation. In normal rats, **1** is metabolized to acylglucuronides, which are secreted into bile, but a portion of the administered dose is secreted into bile intact. In mutant rats (Gunn rats) lacking bilirubin glucuronyl transferase, **1** was excreted efficiently in bile in unchanged form, unlike the parent with a methylene group at C(10). Thus, introduction of the oxygen function at C(10) has little effect on hepatic uptake but a dramatic effect on canalicular secretion into bile.

Introduction

Biliverdin is a blue–green pigment formed in plant and animal metabolism by oxidative cleavage of the heme porphyrin macrocycle (Figure 1).^{1–3} In mammals, biliverdin is reduced rapidly and efficiently by biliverdin reductase to bilirubin, which

is yellow–orange, cytotoxic,⁴ and a powerful antioxidant.⁵ A healthy adult human produces about 250 mg of bilirubin per day, principally from the breakdown of red blood cells. Normally, bilirubin is converted enzymatically in the liver to mono- and di-glucuronide conjugates that are eliminated efficiently in bile.^{1,6} Translocation of bilirubin glucuronides from the liver into bile across the canalicular membrane of the hepatocyte is believed to be effected by the ATP-dependent

[†] University of Nevada.

[‡] University of California.

(1) McDonagh, A. F. *Bile Pigments: Bilatrienes and 5, 15-Biladienes*. In *The Porphyrins*; Dolphin, D., Ed.; Academic Press: New York, 1979; Vol VI, Chapter 6.

(2) Falk, H. *The Chemistry of Linear Oligopyrroles and Bile Pigments*; Springer-Verlag, NY, 1989.

(3) Gossauer, A. *Chimia* **1994**, *48*, 352–361.

(4) (a) Brodersen, R.; Stern, L. *Acta Paediatr. Scand.* **1990**, *79*, 12–19.

(b) Bratliid, D. *Clin. Perinatol.* **1990**, *17*, 449–465. (c) Wennberg, R. P. *NY State J. Med.* **1991**, *91*, 493–496.

(5) (a) Dennery, P. A.; McDonagh, A. F.; Spitz, D. R.; Rodgers, P. A.; Stevenson, D. K. *Free Radical Biol. Med.* **1995**, *19*, 395–404. (b) Llesuy, S. F.; Tomaro, M. L. *Biochim. Biophys. Acta* **1994**, *1223*, 9–14. (c) Neuzil, J.; Stocker, R. *J. Biol. Chem.* **1994**, *269*, 16712–16719.

(6) Chowdhury, J. R.; Wolkoff, A. S.; Chowdhury, N. R.; Arias, I. M. In *The Metabolic and Molecular Bases of Inherited Disease*; Scriver, C. R., Beaudet, A. L., Sly, W. S., Valle, D., Eds.; McGraw-Hill Inc.: New York, 1995; Vol. II, pp 2161–2208.

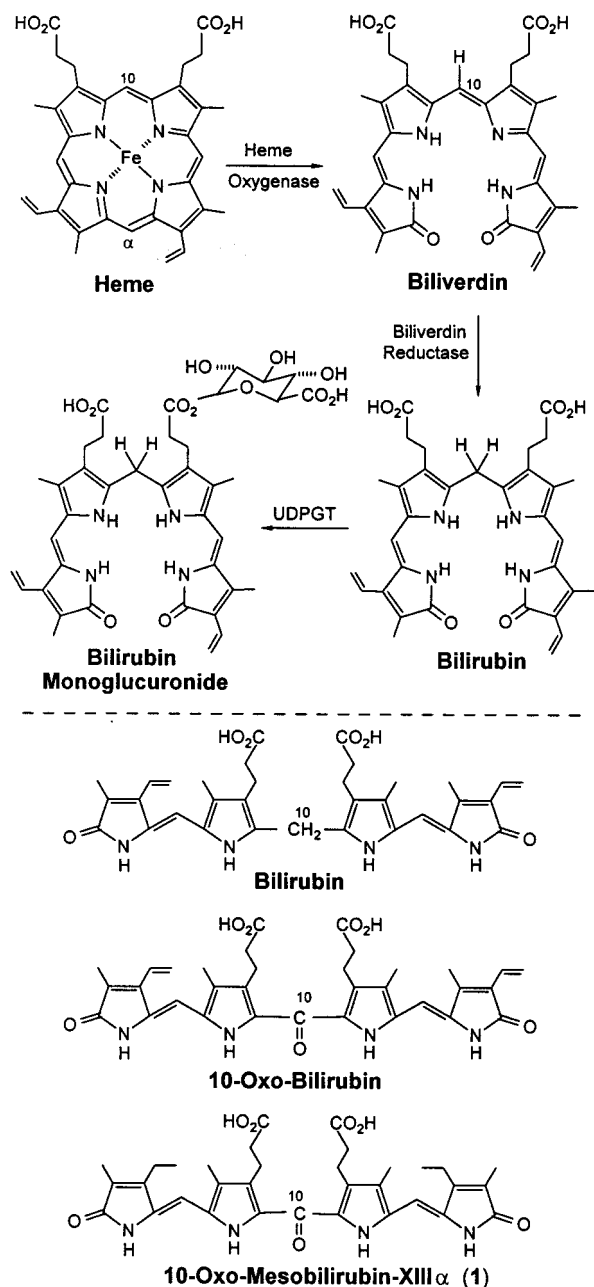


Figure 1. (Upper) Enzymic conversion of heme to (blue-green) biliverdin and (yellow-orange) bilirubin and formation of bilirubin glucuronide, an essential step in the hepatic elimination of bilirubin. The structures are drawn in a porphyrin-like shape. (Lower) Linear representations of bilirubin, 10-oxo-bilirubin, a suggested metabolite in alternate pathways of bilirubin elimination, and its synthetic analogue, 10-oxo-mesobilirubin-XIII α (1).

glycoprotein MRP-2 (multi-drug resistance protein 2; also known as *c*-MOAT, canalicular multi-specific organic anion transporter).⁷ Bilirubin itself is hydrophobic and is not excreted significantly in bile or urine. Presumably, this is because of its high affinity for serum and hepatic proteins and/or because it is not transported by any of the several membrane transport proteins that facilitate the biliary excretion of other organic anions and amphipathic small molecules.

Accumulation of bilirubin or its glucuronides in the body, because of impaired excretion or defective glucuronidation,

(7) (a) Paulusma, C.; Oude Elferink, R. P. J. *J. Mol. Med.* **1997**, *75*, 420–428. (b) Jedlitsky, G.; Leier, I.; Buchholtz, U.; Hummel Eisenbeiss, J.; Burchell, B.; Keppler, D. *Biochem. J.* **1997**, *327*, 305–310.

causes hyperbilirubinemia and jaundice.^{1,6,8} Impaired excretion of bilirubin glucuronides occurs in many types of hepatobiliary disease, whereas deficient glucuronidation, leading to unconjugated hyperbilirubinemia, is seen most commonly in newborn babies and in people with the benign Gilbert's syndrome.^{6,8} However, a total inability to conjugate bilirubin, though it leads to severe hyperbilirubinemia and jaundice and often to neurological damage, does not completely block bilirubin elimination. For example, in some patients with Type I Crigler-Najjar syndrome, or in the homozygous mutant Gunn rat, blood levels of bilirubin reach a steady-state despite constant bilirubin production and a complete lack of bilirubin conjugating activity in the liver and complete absence of bilirubin glucosyl conjugates from bile or urine. Thus, Crigler-Najjar patients and Gunn rats are able to eliminate bilirubin via unknown pathways that do not involve glucuronidation.^{6,8–10} The contribution of these alternate pathways to bilirubin turnover in jaundiced infants is unknown, but obviously, an ability to safely stimulate them would be a boon to the management of neonatal jaundice.

There is some evidence that the alternate pathways of bilirubin elimination are, at least in part, oxidative in nature, possibly involving superoxide or one of the hepatic microsomal cytochrome P-450 enzymes.^{9,10} In the early 1980s, Manitto et al.¹¹ suggested that these pathways might involve production of 10-oxo-bilirubin (Figure 1). The same compound had been suggested earlier as being formed, by an unlikely sequence of reactions, during photodegradation or alkaline decomposition of bilirubin, but it was not characterized or identified.¹² Although Manitto et al. were apparently able to make 10-oxo-bilirubin dimethyl ester in very low yield by reaction of biliverdin dimethyl ester with potassium superoxide in dimethyl sulfoxide, they could not prepare the corresponding free acid. Consequently, the chemical, spectroscopic, and biological properties of this potential bile pigment metabolite remain unknown. In particular, it is not known whether such a metabolite, if formed, would be a substrate of the specific glucuronosyl transferase isozyme that glucuronidates bilirubin or whether it would be secreted *intact* via the liver into bile.¹³ The compound is also of interest as a potential biliverdin reductase inhibitor.

These considerations led us to develop a synthesis of 10-oxo-mesobilirubin-XIII α (1, Figure 1), which is a very close analogue of what would be the natural product, and to study its metabolic disposition in normal rats and in homozygous Gunn rats lacking bilirubin conjugating activity. To our knowledge, this is the first synthesis of a 10-oxo-bilirubin.

Results and Discussion

Synthesis. 10-Oxo-mesobilirubin-XIII α (1) was chosen as a synthetic target because of its symmetry, and because the parent (mesobilirubin-XIII α) has chemical properties very similar to those of bilirubin and, as we shall show, behaves very much like bilirubin *in vivo*.

(8) Schmid, R.; McDonagh, A. In *The Metabolic Basis of Inherited Diseases*; Stanbury, J. B., Wyngaarden, J. B., Frederickson, D. S., Eds.; McGraw-Hill: New York, 1978; pp 1221–1257.

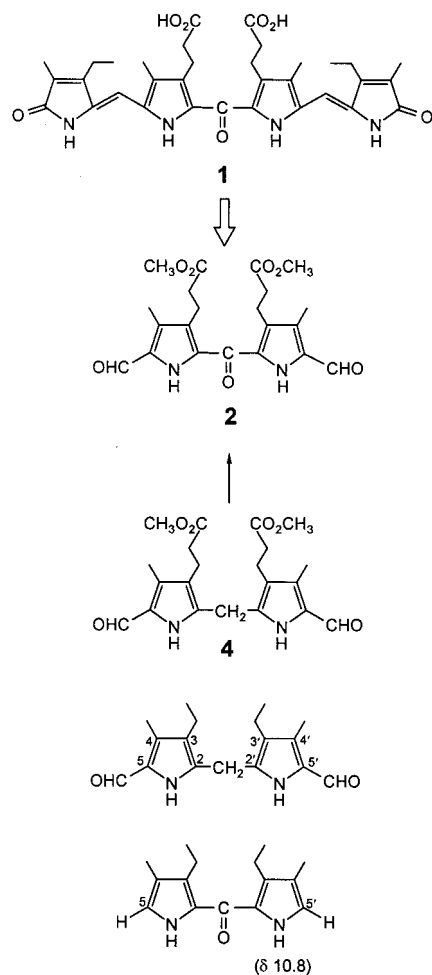
(9) Schmid, R.; Hammaker, L. J. *Clin. Invest.* **1963**, *42*, 1720–1734. (10) For a recent summary, see Tiribelli, C.; Ostrow, J. D. *Hepatology* **1993**, *17*, 715–736.

(11) Galliani, G.; Monti, D.; Speranza, G.; Manitto, P. *Tetrahedron Lett.* **1984**, *25*, 6037–6040.

(12) Ostrow, J. D. *Semin. Hematol.* **1972**, *9*, 113–125.

(13) (a) McDonagh, A. F.; Lightner, D. A. In *Hepatic Metabolism and Disposition of Endo and Xenobiotics*; Falk Symposium No. 57; Bock, K. W., Gerok, W., Matern, S., Eds.; Kluwer: Dordrecht, The Netherlands, 1991; Chapter 5, pp 47–59. (b) McDonagh, A. F.; Lightner, D. A. *Cell. Mol. Biol.* **1994**, *40*, 965–974. (c) For leading references, see Tiribelli, C.; Ostrow, J. D. *Hepatology* **1996**, 1296–1311.

Scheme 1



We were attracted to the possibility of preparing 10-oxo-rubins from an oxygenated dipyrrole core by a [1 + 2 + 1] condensation of an oxo-dipyrrole such as **2** (Scheme 1) with a suitable pyrrolinone. A similar approach has been used successfully in the preparation of bilirubins from dipyrrole-methanes,^{2,14} and it offers the attraction that a family of 10-oxo-rubins might be prepared from dipyrrole ketone **2** and a variety of differently substituted pyrrolinones. For the synthesis of **2**, we turned to the work of Clezy et al.¹⁵ and Paine and Dolphin,¹⁶ who described various methods for converting dipyrrole-methanes into dipyrrole ketones. One such oxidation was reported using a combination of $\text{Pb}(\text{OAc})_4$ and PbO_2 , but the yields were variable and low and the reaction times were long.¹⁵ Another used SO_2Cl_2 to convert the central CH_2 to CCl_2 , followed by hydrolysis to give the ketone.¹⁵ This route appeared particularly attractive because it would afford **2** by a series of known reactions. However, dipyrrole-methane dialdehyde **4**, obtained in high yield from the corresponding readily available dipyrrole-methane tetraester, in our hands gave only a trace of the corresponding dipyrrole-methane and none of the desired oxo-dipyrrole upon reaction with SO_2Cl_2 . Repeating the reaction after protecting the sensitive aldehyde groups as their condensation production with methyl cyanoacetate gave only a few percent yield of the desired oxo compound.

Seeking a higher yield alternative, we considered the prospect of introducing the oxo group by oxidation with ceric ammonium

nitrate (CAN).^{16,17} In a trial run, direct reaction of the simpler 3,3'-diethyl-4,4'-dimethyldipyrrole-methane dialdehyde of Scheme 1 disappointingly failed to give the expected oxo product. Following an alternative route, CAN oxidation of the corresponding diester (5,5'-dicarboethoxy)^{17c} afforded the oxo-diester in 92% yield. This was saponified to the diacid in 90% yield and decarboxylated to give the 5H,5'H-dipyrrole ketone of Scheme 1 in 70% yield. Unfortunately, the ketone resisted our attempts to achieve formylation at positions 5 and 5'.

Drawing from our experience in CAN oxidations of pyrrole esters^{17a} and dipyrrole-methane diesters,^{17c} we surmised that the CAN oxidations of the simple dipyrrole-methane dialdehyde had failed because it was too insoluble in the aqueous acetic acid-THF reaction solvent. Previous experience had indicated that the presence of propionic acid ester groups offered improved solubility and higher yields in CAN oxidations,^{17c} and so we suspected that their presence might also have influenced the course of the attempted conversion ($\text{CH}_2 \rightarrow \text{CCl}_2 \rightarrow \text{C}=\text{O}$) with SO_2Cl_2 . Our expectations were thus realized: reaction of **4** with CAN (Scheme 2), using improvements in the solvent system, produced **2** in good yield, whereas other oxidants ($\text{SO}_2\text{Cl}_2/\text{HOAc}$ or $\text{SO}_2\text{Cl}_2/\text{CHCl}_3$ or $\text{Pb}(\text{OAc})_4$ and PbO_2) failed.

This allowed us to prepare the desired dipyrrole ketone dialdehyde **2** in four steps from monopyrrole **7**, whose diester groups were differentiated as methyl and the more easily deprotected *tert*-butyl types (synthetic Scheme 2). Oxidation of **7** with $\text{Pb}(\text{OAc})_4$ proceeded in high yield to afford the acetoxy diester (**6**), which was solvolysed in aqueous acetic acid to afford the dipyrrole-methane (**5**) in excellent yield. The *tert*-butyl esters were hydrolyzed and decarboxylated in TFA, and the intermediate α -free dipyrrole-methane was smoothly formylated in situ using methyl orthoformate to afford dialdehyde **4** in high yield. Oxidation using CAN gave the required dipyrrole ketone (**2**) in 52% yield (30% overall from **7**).

For completion of the synthesis of 10-oxo-rubin **1** from **2**, ample quantities of pyrrolinone **3** were required. Synthesis of **3** was accomplished in six steps, as outlined in Scheme 3, using the Barton-Zard pyrrole synthesis.¹⁸ The target intermediate, tosylpyrrole **8** was prepared from 2-nitro-3-acetoxypentane by reaction with *p*-toluenesulfonylmethyl isocyanide (TosMIC), an expensive, though readily synthesized reactant. We modified the TosMIC preparation reported in *Organic Synthesis*¹⁹ and doubled the yield, from 42.47% to 85% (see Experimental section). We also found that tosylpyrroles can be brominated in high yield using Br_2 in place of the recommended phenyltrimethylammonium bromide perbromide. Thus **8** was converted to **9** in excellent yield, and **9** was converted to tosylpyrrolinone **10** in high yield by reaction with aqueous TFA. Removal of the tosyl group using NaBH_4 was achieved smoothly to afford **3** in 90% yield (35% overall yield from nitroethane). The indicated modifications constitute an overall improvement in the Barton-Zard pyrrole synthesis and provide a facile, high-yield procedure for the production of **3**. Reaction of a 10-fold molar excess of **3** with dipyrrole **2** afforded the desired 10-oxo-mesobilirubin-XIII α (**1**) in 77% yield (23% overall from

(17) (a) Thyraan, T.; Lightner, D. A. *Tetrahedron Lett.* **1995**, *36*, 4345–4348. (b) Thyraan, T.; Lightner, D. A. *Tetrahedron Lett.* **1996**, *37*, 315–318. (c) Thyraan, T.; Lightner, D. A. *J. Heterocycl. Chem.* **1996**, *33*, 221–222.

(18) (a) Barton, D. H. R.; Zard, S. Z. *J. Chem. Soc., Chem. Commun.* **1985**, 1098–1100. (b) Barton, D. H. R.; Kervagoret, J.; Zard, S. Z. *Tetrahedron* **1990**, *46*, 7587–7598.

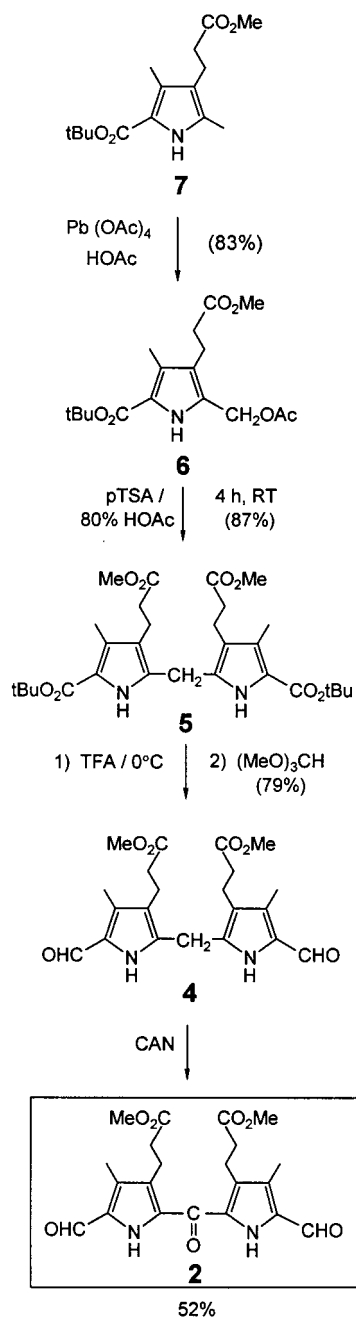
(19) (a) Hoogenboom, B. E.; Oldenzel, O. H.; van Leusen, A. M. *Org. Synth.* **1988**, Coll. Vol. 6, 987–990. (b) See also, van Leusen, A. M. *Org. React.* **1999**, accepted for publication.

(14) Boiadjev, S. E.; Lightner, D. A. *SYNLETT* **1994**, 777–785.

(15) Clezy, P. S.; Liepa, A. J.; Nichol, A. W.; Smythe, G. A. *Aust. J. Chem.* **1970**, *23*, 589–602.

(16) Paine, J. B.; Dolphin, D. *Can. J. Chem.* **1976**, *54*, 411–414.

Scheme 2

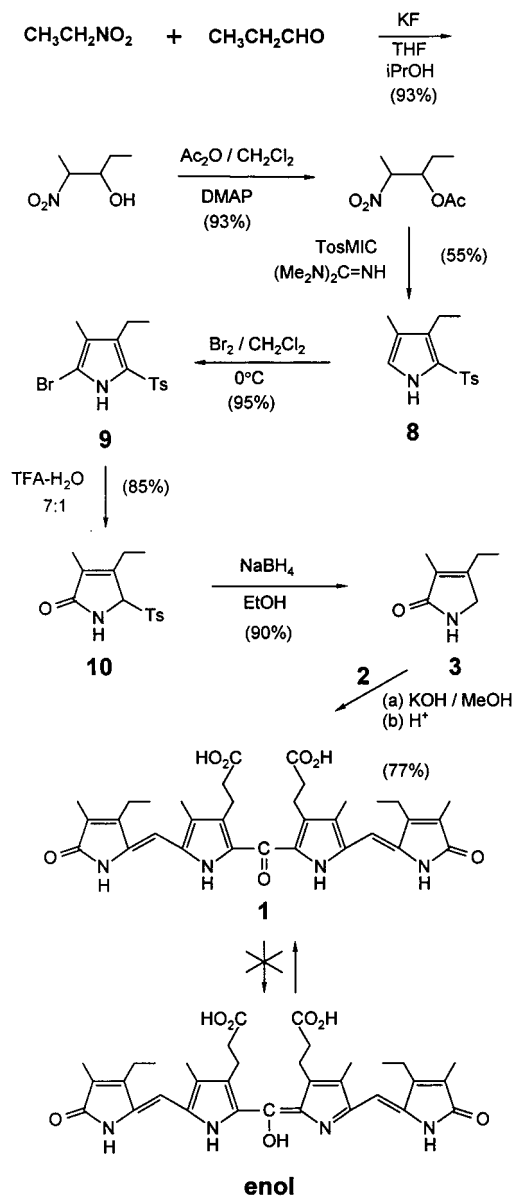


7) as an orange-red solid. In the absence of a large excess of 3, the yield of 1 was lowered and monocoupled product was isolated.

Molecular Structure. The constitutional structure of 1 follows from the structures of the mono and dipyrrole synthetic precursors and is confirmed by its NMR spectral data (compared in Table 1 with NMR data from the parent, mesobilirubin-XIII α). The ¹³C NMR data for 1 and mesobilirubin-XIII α are nearly identical, differing most significantly at C(10), where the CH₂ of the latter has been replaced by a C=O in the former. The ¹³C NMR chemical shift of C(10) in 1 is more like that of a vinylogous amide than a ketone. Pyrrole ring carbons nearest C(10), notably C(9)/C(11), are not much affected, but those at alternant sites [C(8)/C(12), C(6)/C(14), C(4)/C(16), and C(2)/C(18)] experience a much stronger deshielding relative to the parent than do the nonalternant carbons.

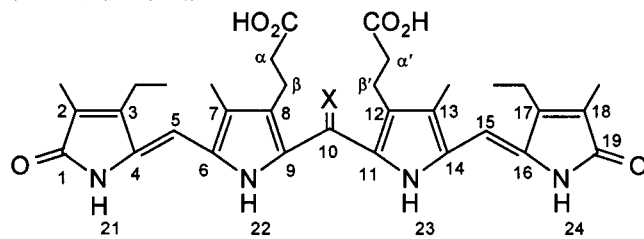
The ¹H NMR of 1 is also consistent with the constitutional structure shown. In (CD₃)₂SO solvent, only small chemical shift

Scheme 3

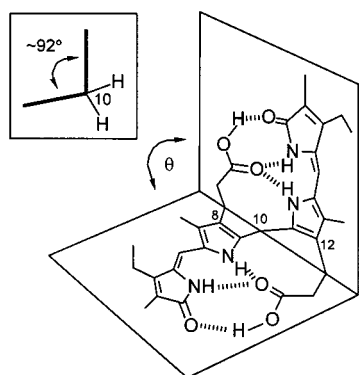


differences are found for most C-Hs when compared to the parent, mesobilirubin-XIII α , except for the absence of the C(10) CH₂ signals. Presumably, the somewhat more deshielded resonances for the α,α' -CH₂, β,β' -CH₂ of 1 are due to the close proximity of the C(10)=O. Both the lactam (especially) and the pyrrole NHs of 1 are considerably more deshielded than the corresponding NHs of the parent. While the assignment of the pyrrole NH of mesobilirubin-XIII α can be made from its NOE with the C(10) hydrogens, the assignment in 1 was made by comparison with the pyrrole NH chemical shifts of the model 5H,5'H-dipyrrole ketone (Scheme 1), determined in (CD₃)₂SO. We found no evidence for tautomerism to the enol form (Scheme 3).

Although the NMR data for 1 are consistent with the constitutional structure shown, its conformation is difficult to determine. As is typical of bilirubins, the dipyrinones of 1 adopt a *syn*-4Z, (*syn*-15Z) configuration, as indicated by NOEs between C(5)-H and the C(7)-CH₃ and C(3)-CH₂ groups (or between C(15)-H and the C(13)-CH₃ and C(17)-CH₂ groups) measured in (CD₃)₂SO. Unlike mesobilirubin-XIII α , the pigment was surprisingly *insoluble* in CDCl₃, too insoluble for NOE studies, or for an examination of the proton coupling constants

Table 1. Comparison of ^1H - and ^{13}C NMR Chemical Shifts for 10-Oxo-mesobilirubin-XIII α (1, X = O) and Mesobilirubin-XIII α (X = H,H) in $(\text{CD}_3)_2\text{SO}$ at 23 °C


position	^1H NMR signal		^{13}C NMR signal	
	X=O	X=H ₂	X=O	X=H ₂
2,18			126.0	122.5
2,18-CH ₃	1.75	1.78	8.31	9.14
1,19-C=O			172.8	171.9
3,17			147.7	147.2
3,17-CH ₂ CH ₃	2.52	2.50	17.46	17.15
3,17-CH ₂ CH ₃	1.07	1.09	14.85	14.81
4,16			133.6	127.8
5,15-CH=	5.97	5.94	96.40	97.69
6,14			129.2	122.0
7,13			122.9	122.9
7,13-CH ₃	2.07	2.00	9.38	8.07
8,12			128.2	119.2
β,β' -CH ₂	2.69	2.43	20.59	19.25
α,α' -CH ₂	2.31	2.00	35.03	34.34
α,α' -COOH	12.00	11.83	174.1	174.0
9,11			131.6	130.3
10		2.95	176.0	23.46
21,24-NH	10.20	9.27		
22,23-NH	10.89	10.27		

**Figure 2.** Lowest-energy dominant conformation of mesobilirubin-XIII α , shaped like a ridge-tile and stabilized by a network of 6 hydrogen bonds shown in dashed lines. (Inset) Edge view of the ridge-tile showing the C(10) hydrogens. Computations using Sybyl give $\theta \sim 92^\circ$, smaller than that ($\theta \sim 104^\circ$) found in a crystal of mesobilirubin-IX α chloroform solvate, where packing forces may come into effect. (Becker, W.; Sheldrick, W. S. *Acta Crystallogr., Sect. B* **1978**, *34*, 1298–1304.)

within the $\text{CH}_2\text{CH}_2\text{CO}_2\text{H}$ segments, or even for measuring the NH chemical shifts, all of which have served to probe and confirm the secondary structures of bilirubins in solution.²⁰ For bilirubin and mesobilirubin-XIII α , the dominant conformation is shaped like a ridge-tile (although the structure is not rigid) and stabilized by a network of six intramolecular hydrogen bonds (Figure 2).

Conformation from Molecular Dynamics. Absent the customary NMR data useful for eliciting the conformation of bilirubins in nonpolar solvents, we turned to an analysis of the

secondary structure of **1** by molecular dynamics calculations using Sybyl. Such analyses have proved instructive in previous studies^{20,21} and found to be quite accurate for bilirubin and mesobilirubin-XIII α .²²

Using the Tripos force field in Sybyl, conformational energy maps (Figure 3) were constructed by rotating the dipyrri- none units of **1** independently about the C(9)–C(10) and C(10)–C(11) bonds, corresponding to torsion angles ϕ_1 and ϕ_2 , respectively, as was done earlier for mesobilirubin-XIII α .²² With ϕ_1 and ϕ_2 defined as 0° in a porphyrin-like conformation (Figure 1), a large array of conformations can be created through rotations about ϕ_1 and ϕ_2 , including the linear conformation (Figure 1) with $\phi_1 = \phi_2 = 180^\circ$. Figure 3 shows a mapping of conformational energy vs rotation angles, ϕ_1 and ϕ_2 , for **1**. Some conformations, most notably the ridge-tile conformations, are considerably stabilized through intramolecular hydrogen bonding.²³ Molecular dynamics calculations find global energy minima corresponding to identical enantiomeric structures for **1** (Figure 4), with each enantiomer being represented by several different wells on the surfaces of Figure 3. Thus, isoenergetic global minima are found for identical *M*-helicity conformations near $(\phi_1, \phi_2) \sim (-60^\circ, -60^\circ)$, $(+300^\circ, -60^\circ)$, $(-60^\circ, +300^\circ)$, and $(+300^\circ, +300^\circ)$ and for the isoenergetic *P*-helicity conformer located near $(\phi_1, \phi_2) \sim (+60^\circ, +60^\circ)$. Through the action of intramolecular hydrogen bonding, the molecule adopts one basic three-dimensional molecular structure corresponding to the cited minima, a conformation where the two dipyrri- none chromophores lie in nearly orthogonal planes with dihedral angles of 89° in **1** and 92° in mesobilirubin-XIII α . Local minima are found lying nearby the global minima; for example, $\phi_1 \sim +80^\circ$, $\phi_2 \sim +170^\circ$ and $\phi_1 \sim +160^\circ$, $\phi_2 \sim +90^\circ$ lie near the global minimum at $\phi_1 = \phi_2 \sim +60^\circ$ and some 12.5 kcal/mol higher energy. These local minima have a conformation that allows only 3 intramolecular hydrogen bonds. In contrast, the porphyrin-like and linear shapes are much higher energy: 24 kcal/mol for the former, 38 kcal/mol for the latter, relative to the global minimum.

The interconversion of *M* and *P* enantiomers of **1** can be tracked on the conformational energy map (Figure 3), as discussed previously for mesobilirubin-XIII α .²² In fact, the *M* and *P* conformational enantiomers of **1** (Figure 4) interconvert over a barrier calculated to be significantly nearly the same (17–23 kcal/mol) as those of the parent rubin (19–22 kcal).²³ The interconversion occurs by breaking 3–4 hydrogen bonds while the dipyrri- none are rotated about ϕ_1 and ϕ_2 , then remaking the hydrogen bonds.²³ From an examination of Figure 2, two distinct low-energy interconversion pathways are found in **1** to take the *P*-helicity conformer to the *M*: (i) A route passing through a local minimum from $(\phi_1 = \phi_2 \sim 60^\circ) \rightarrow (\phi_1 \sim 70^\circ, \phi_2 \sim 110^\circ) \rightarrow (\phi_1 \sim -80^\circ, \phi_2 \sim 140^\circ) \rightarrow (\phi_1 \sim 80^\circ, \phi_2 \sim 170^\circ) \rightarrow (\phi_1 \sim 60^\circ, \phi_2 \sim 180^\circ) \rightarrow (\phi_1 \sim 40^\circ, \phi_1 \sim 200^\circ) \rightarrow (\phi_1 \sim 20^\circ, \phi_2 \sim 220^\circ) \rightarrow (\phi_1 \sim 0^\circ, \phi_2 \sim 230^\circ) \rightarrow (\phi_1 \sim -20^\circ, \phi_2 \sim 270^\circ)$ and down to $(\phi_1 \sim -60^\circ, \phi_2 \sim 300^\circ)$ with an activation barrier of ~ 17 kcal/mol. (ii) A route from $(\phi_1 = \phi_2 \sim 60^\circ) \rightarrow (\phi_1 \sim 60^\circ, \phi_2 \sim 20^\circ) \rightarrow (\phi_1 \sim 40^\circ, \phi_2 \sim 10^\circ) \rightarrow (\phi_1 \sim 20^\circ, \phi_2 \sim 0^\circ) \rightarrow (\phi_1 \sim 10^\circ, \phi_2 \sim -10^\circ) \rightarrow (\phi_1 \sim 10^\circ, \phi_1 \sim -20^\circ) \rightarrow (\phi_1 \sim -50^\circ, \phi_2 \sim -30^\circ)$ and down to $(\phi_1 \sim -60^\circ, \phi_2 \sim -60^\circ)$ with a barrier of ~ 23 kcal/mol. The relative energies (kcal/mole) associated with path (i) are $0 \rightarrow 10.7 \rightarrow 15.6 \rightarrow 12.4$ (local

(21) (a) Kar, A.; Lightner, D. A. *Tetrahedron* **1998**, *54*, 12671–12690.(b) Kar, A.; Lightner, D. A. *J. Heterocyclic Chem.* **1998**, *35*, 795–803. (c) Kar, A.; Lightner, D. A. *Tetrahedron: Asymmetry* **1998**, *9*, 3864–3880.(22) Person, R. V.; Peterson, B. R.; Lightner, D. A. *J. Am. Chem. Soc.* **1994**, *116*, 42–59.(23) Boiadjev, S. E.; Pfeiffer, W. P.; Lightner, D. A. *Tetrahedron* **1997**, *53*, 14547–14564.(20) (a) Boiadjev, S. E.; Lightner, D. A. *Tetrahedron: Asymmetry* **1996**, *7*, 1309–1322. (b) Boiadjev, S. E.; Lightner, D. A. *Tetrahedron: Asymmetry* **1997**, *8*, 2115–2129. (c) Kar, A.; Lightner, D. A. *Tetrahedron* **1998**, *54*, 5151–5170.

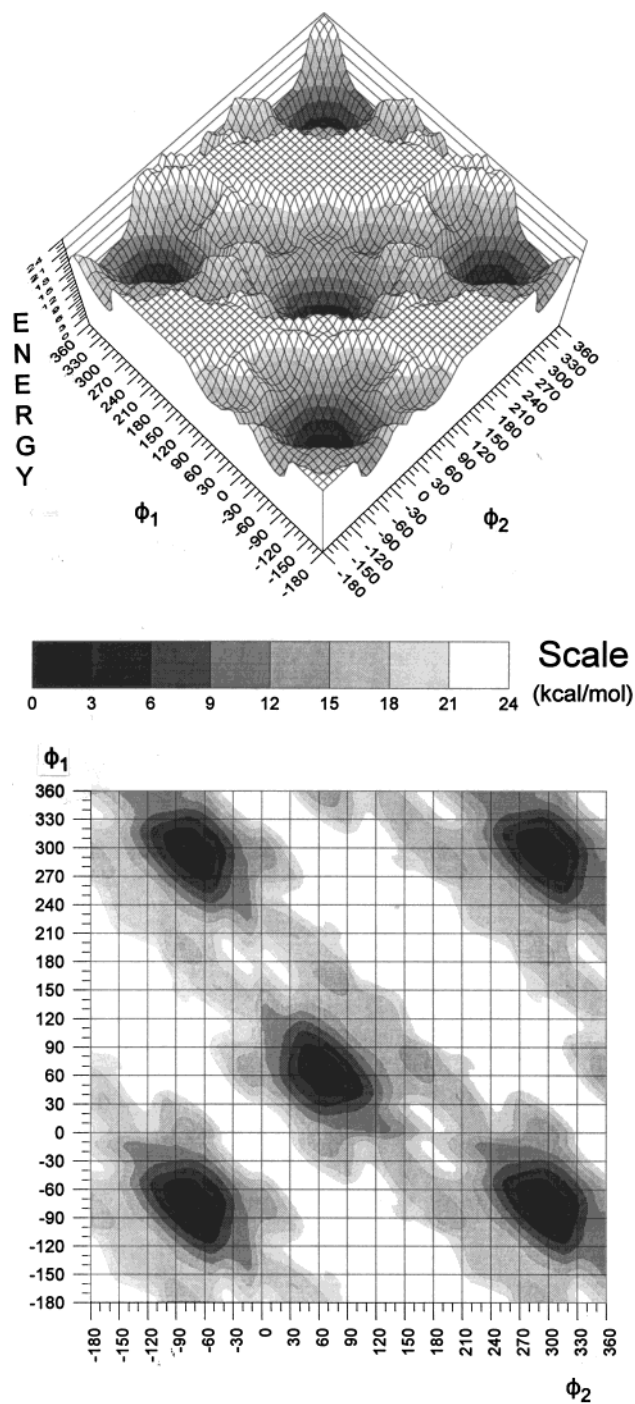


Figure 3. (Upper) Potential energy surface and (Lower) contour map for 10-oxo-rubin (**1**) conformations generated by rotating the two dipyrri-*n*one groups independently about the C(9)–C(10) and C(10)–C(11) bonds ϕ_1 and ϕ_2 , respectively. The energy scale (Middle) is in kcal/mol, and global minima (set to 0 kcal/mol) are found near $(\phi_1, \phi_2) \sim (-60^\circ, -60^\circ)$, $(-60^\circ, 300^\circ)$, $(300^\circ, -60^\circ)$, and $(300^\circ, 300^\circ)$ (*M*-chirality) and near $(\phi_1, \phi_2) \sim (+60^\circ, +60^\circ)$ (*P*-chirality).

minimum) $\rightarrow 13.4 \rightarrow 14.6 \rightarrow 15.6 \rightarrow 17.2 \rightarrow 10.5 \rightarrow 7.2 \rightarrow 0.0$; those for path (ii) are $0.0 \rightarrow 8.0 \rightarrow 15.2 \rightarrow 23.2 \rightarrow 18.6 \rightarrow 23.2 \rightarrow 12.8 \rightarrow 0.0$. The presence of the C(10)=O group of **1** appears to induce relatively little change in the interconversion barriers and pathways between the *M* and *P* ridge-tiles of the parent, mesobilirubin-XIII α .

Unlike the parent, however, whose intramolecularly hydrogen bonded global minimum has nearly the same ridge-tile shape as the non-hydrogen-bonded global minimum,²³ the conformation of the non-hydrogen-bonded global minimum of **1** (Figure

5) differs significantly from that of the intramolecularly hydrogen bonded minima of Figure 4 (right). The non-hydrogen-bonded global minimum of **1** (Figure 5) shows the pigment having adopted a helical, porphyrin-like conformation with significant twisting in each dipyrri-*n*one. The net result is that intramolecular hydrogen bonding is not as stabilizing in **1** as it is in the ridge-tile parent. Whether this is due to the sp^2 hybridization at C(10) of **1** or to dipole interactions from the C=O bond is not clear. However, it may be relevant that the non-hydrogen-bonded conformation of **1** looks like a hybrid of that found in the parent (mesobilirubin-XIII α), which has C(10) sp^3 hybridized, and that found in mesobiliverdin-XIII α , which has C(10) sp^2 hybridized (Figure 5). Absent intramolecular hydrogen bonding, the planar dipyrri-*n*ones of **1** become twisted, and the torsion angles about C(10) are reduced greatly. Such a relaxed, non-hydrogen-bonded conformation is more helical than that found in mesobiliverdin-XIII α , which also has an sp^2 C(10) but which derives most of its helicity from twisting within the dipyrri-*n*ones (Table 2).

Optical Spectra. Oxo-rubin **1** is noticeably *red*, whereas its parent rubin is *yellow*. Its UV–vis spectra in chloroform and dimethyl sulfoxide (Figure 6) show considerable broadening and hypochromism of the intense ~ 430 nm long wavelength absorption band of the parent, mesobilirubin-XIII α . At least two long wavelength absorptions are seen for **1**, one near 380 nm and a broader band near 440 nm. It is the latter, tailing off toward 500 nm, that is associated with the bright red–orange color of **1**. Solutions of oxo-rubin **1** also behave differently from its parent rubin upon basification or acidification (Figure 6). In aqueous sodium hydroxide, the red color of **1** intensified, while in the parent there is little color change. In the latter, the band center shifts to ~ 400 nm, while in **1** the 380 nm band intensifies and shifts to 395 nm, and the broad band near 450 nm shifts to ~ 530 nm and weakens. Presumably, the spectral changes seen in **1** reflect more than the simple deprotonation of propionic acid groups expected in both pigments, and they may indicate the formation of the C(10) enolate of **1**. In trifluoroacetic acid, the spectra differ again. The ~ 530 nm weak band seen for **1** in aqueous NaOH is also found in TFA, but intensified, while the intense ~ 395 nm band shifts to ~ 360 nm and weakens somewhat. In contrast, in mesobilirubin-XIII α , the ~ 400 nm band separates with added TFA into two intense bands, one near 425 nm and one near 480 nm, and the solution is red. In TFA, the C(10) carbonyl of **1** may be in the enol form, and enolization may also be present at the lactam carbonyls. The latter might account for the spectral shifts seen in the parent.

In the presence of chiral complexation agents, including serum albumin, bilirubin and mesobilirubin-XIII α give intense bisignate circular dichroism (CD) Cotton effects for the long wavelength absorption near 430–450 nm.^{24,25} The CD spectra have been interpreted in terms of exciton coupling between the two dipyrri-*n*one chromophores, and the exciton chirality rule²⁶ has been used to assign the absolute stereochemistry of the predominant ridge-tile enantiomer (*M* or *P*, as in Figure 4).^{22,24a} Oxo-rubin **1**, like its parent, gives a well-defined, strong

(24) (a) Lightner, D. A.; Gawroński, J. K.; Wijekoon, W. M. D. *J. Am. Chem. Soc.* **1987**, *109*, 6354–6362. (b) Lightner, D. A.; An, J. Y.; Pu, Y. M. *Arch. Biochem. Biophys.* **1988**, *262*, 543–559. (c) Lightner, D. A.; Wijekoon, W. M. D.; Zhang, M. H. *J. Biol. Chem.* **1988**, *263*, 16669–16676. (d) Gawroński, J. K.; Polonski, T.; Lightner, D. A. *Tetrahedron* **1990**, *46*, 8053–8066.

(25) (a) Kano, K.; Arimoto, S.; Ishimura, T. *J. Chem. Soc., Perkin Trans. 2* **1995**, 1651–1666. (b) Kano, K.; Tsujino, N.; Kim, M. *J. Chem. Soc., Perkin Trans. 2* **1992**, 1747–1752.

(26) Harada, N.; Nakanishi, K. *Circular Dichroism Spectroscopy-Exciton Coupling in Organic Stereochemistry*; University Science Books: Mill Valley, CA, 1983.

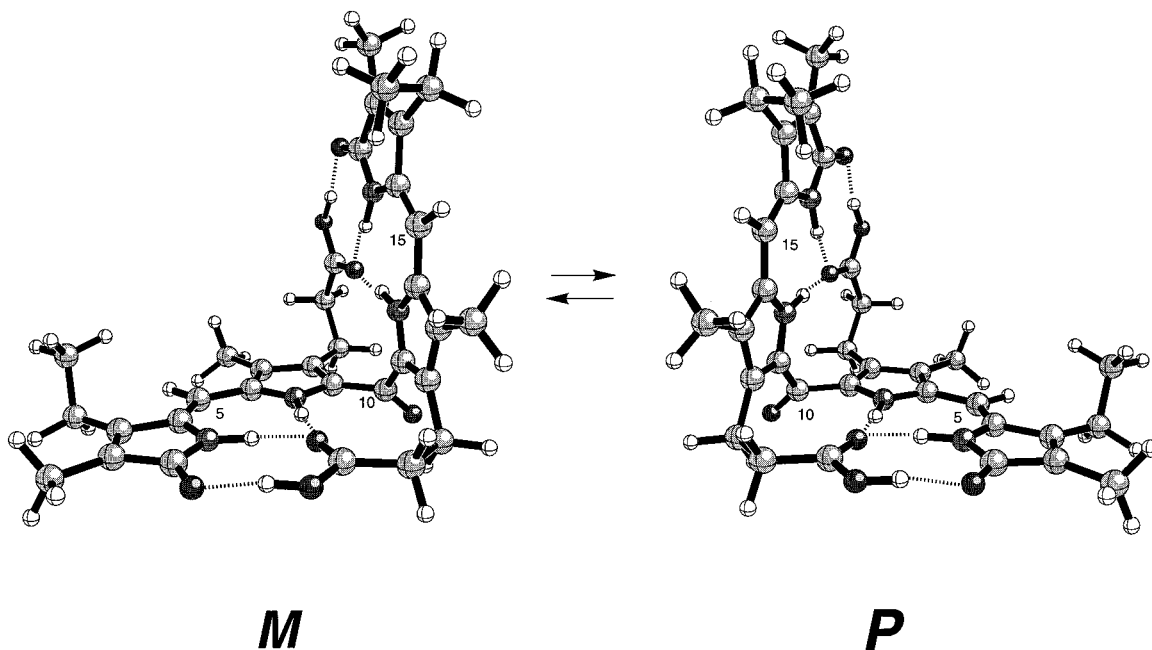


Figure 4. Ball and stick conformational representations for the ridge-tilt shape *M* and *P* intramolecularly hydrogen-bonded enantiomers of **1**.

bisignate CD spectrum ($\Delta\epsilon_{376}^{\max} -28.5$, $\Delta\epsilon_{321}^{\max} +37.5$) in pH 7.8 aqueous buffered human serum albumin (HSA) (Figure 7). Unexpectedly, the CDs of the two pigments are opposite in sign and differ in magnitude and band center. For the oxo-rubin, the predominant enantiomer in the bound state has *M*-helicity, whereas the parent mesobilirubin-XIII α in the bound state has predominantly *P*-helicity.

Solution and Chromatographic Properties. Unlike the bright yellow parent, mesobilirubin-XIII α , oxo-rubin **1** is a bright red–orange solid that forms red–orange solutions. It is noticeably and surprisingly less soluble than its parent in organic solvents such as chloroform, dichloromethane, and acetone. This apparent increase in polarity can also be seen in a comparison of their chromatographic behavior. Oxo-rubin **1** has an $R_f \sim 0.25$ on silica gel TLC using 4% by vol. CH₃OH in CH₂Cl₂ as eluent; whereas the parent rubin exhibits an $R_f \sim 0.85$. On reverse-phase HPLC,²⁷ **1** has a retention time of ~ 8.2 min vs ~ 18.3 for the parent. Typically, bilirubin and mesobilirubin do not extract from CHCl₃ into 5% aqueous sodium bicarbonate. Similarly, oxo-rubin **1** is also not extracted into dilute (or saturated) aqueous sodium bicarbonate. The data indicate that, while the change at C(10) of mesobilirubin-XIII α from CH₂ to C=O render the pigment (**1**) redder and more polar than its parent, it does not have a large effect on the chloroform/bicarbonate partition coefficient, and **1** is no more soluble in weak aqueous base. This is consistent with intramolecular hydrogen bonding (Figure 4).

Biological Properties. Figure 8a shows an HPLC chromatogram of bile from a normal rat collected just before ($t = 0$) intravenous injection of a small bolus (0.25 mg) of mesobilirubin-XIII α dissolved in rat serum (1 mL). The tallest, most polar, peak is bilirubin diglucuronide; the two smaller peaks are the two diastereomeric bilirubin monoglucuronides. After injection of mesobilirubin-XIII α , there was a marked increase in peak area at the retention times of the bilirubin diglucuronide peak and the most polar bilirubin monoglucuronide peak. Concomitantly there was a small hypsochromic shift in the absorption spectra corresponding to those peaks. The increase in peak area

was maximal at about 15 min after injection and thereafter decreased asymptotically to zero over the next 45 min. We ascribe the increased peak areas to the diglucuronide and monoglucuronide of mesobilirubin XIII α , which in our HPLC system do not separate, respectively, from the endogenous bilirubin diglucuronide and one of the monoglucuronides of bilirubin. Consistent with this interpretation, hydrolysis of bile samples with NaOH or β -glucuronidase, which is specific for β -glucuronides, resulted in loss of glucuronide peaks and the appearance of both bilirubin and mesobilirubin XIII α . To obtain an approximate biliary excretion profile for the glucuronides of mesobilirubin XIII α , we measured the sum of the peak areas for the bilirubin and mesobilirubin XIII α diglucuronides and the sum of the peak areas for the bilirubin and mesobilirubin monoglucuronides and then subtracted from these the estimated contributions from the bilirubin mono and diglucuronides based on analyses of bile obtained before injection of mesobilirubin XIII α and after elimination of the compound in bile was complete. These biliary excretion profiles are shown in Figure 8b. When mesobilirubin XIII α was injected under similar conditions into homozygous Gunn rats, which lack bilirubin conjugating activity, there was no significant excretion of the compound or colored metabolites of it in bile over a similar time period. We conclude that exogenous mesobilirubin XIII α is metabolized much like endogenous bilirubin in the rat. It is not excreted significantly in bile unchanged but is metabolized to mono and diglucuronides that are excreted promptly in bile, presumably via the MRP-2 (*c*-MOAT) transport system.⁷

In contrast to mesobilirubin-XIII α , oxo-rubin **1** was excreted rapidly in unchanged form in bile after intravenous injection of the same dose in Gunn rats (Figure 9c,d). Similarly, in normal rats with a functional bilirubin conjugating system, a substantial proportion of the injected dose was excreted in bile unchanged, with similar kinetics as in Gunn rats (Figure 9). In normal rats, however, two additional peaks were detected in chromatograms of bile (Figure 9a). These were identified as glucuronides of **1** by hydrolysis with both NaOH and β -glucuronidase, by the observation that they were not formed in Gunn rats, and by their characteristic double-humped UV–vis absorption spectra.

Hepatic Metabolism. Hepatic uptake followed by intrahe-

(27) McDonagh, A. F.; Palma, L. A.; Lightner, D. A. *J. Am. Chem. Soc.* **1982**, *104*, 6867–6869.

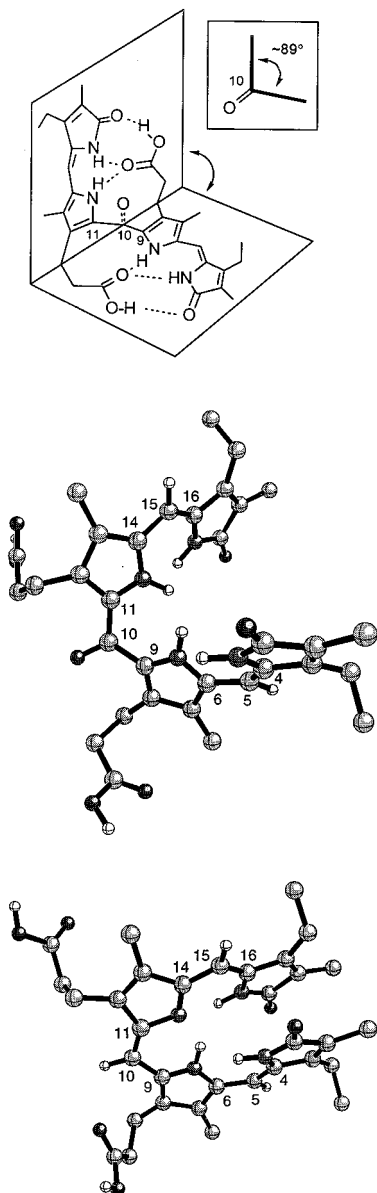


Figure 5. (Top) Lowest-energy dominant conformation of **1**, shaped like a ridge-tile and stabilized by a network of 6 hydrogen bonds shown in dashed lines. The C(10) carbonyl group (C=O) projects behind the two intersecting planes. (Inset) Edge view of the ridge-tile showing the C(10)=O. (Middle and Bottom) Ball and stick representations for (Upper) relaxed, *non-hydrogen-bonded* conformation of oxo-rubin **1**, and (Lower) minimum energy conformation of mesobiliverdin-XIII α .

patic glucuronidation is an important route for the detoxification and disposal of compounds bearing COOH, OH, NH, and SH groups. Although there has been considerable recent progress in elucidating the primary structures of UDP-glucuronosyl transferases,²⁸ the chemical mechanisms of enzymic glucuronidation reactions are still unknown. One endogenous compound that commonly undergoes glycosylation in animals is bilirubin, which is metabolized in mammals principally to two isomeric monoglucuronides and a diglucuronide. In the rat these are essentially the only bilirubin metabolites in nascent bile,

(28) (a) Brierley, C. G.; Burchell, B. *BioEssays* **1993**, *15*, 749–754. (b) Jansen, P. L. M.; Gulder, G. J.; Burchell, B.; Bock, K. W. *Hepatology* **1992**, *15*, 532–544. (c) Tephly, T. F.; Burchell, B. *Trends Pharmacol. Sci.* **1990**, *11*, 276–279.

(29) (a) Ritter, J. K.; Chen, F.; Sheen, Y. Y.; Tran, H. M.; Kimura, S.; Yeatman, M. T.; Owens, I. S. *J. Biol. Chem.* **1992**, *267*, 3257–3261. (b) Sato, H.; Koiwai, O.; Tanabe, K.; Kashiwamata, S. *Biochem. Biophys. Res. Commun.* **1990**, *169*, 260–264.

Table 2. Conformation-Determining Interplanar and Torsion Angles^a for Oxo-Rubin **1** and Mesobiliverdin-XIII α

angle ^a	1 ridge-tile H-bonded	1 relaxed No H bonds	mesobiliverdin-XIII α
interplanar angle ^b , θ	88	40	5.2
torsion angles, ϕ			
6–5=4–21	0.4	3.3	3.1
14–15=16–24	–0.2	3.4	3.7
4=5–6–22	–0.9	36	27
16=15–14–23	–3.4	36	27
11–10–9–22	59	25	4.4
9–10–11–23	60	22	1.3
lactam O to lactam O distance (Å) ^c	9.4	9.1	5.1

^a Values in degrees. ^b Between pyrrole rings. ^c Nonbonded distance O to O.

and unconjugated bilirubin is barely detectable (except as an artifact). Since bilirubin UDP-glucuronosyl transferase has considerable sequence and structural homology to other UDP-glucuronosyl transferases,^{28a,b,29} the chemical mechanisms involved in the glucuronidation of bilirubin are probably similar to those involved in the glucuronidation of other carboxylic acids.

Bilirubin (Figure 1) has to be glucuronidated for excretion because it both is lipophilic and binds with high affinity to serum albumin and to proteins in the liver. The same is true for mesobiliverdin-XIII α (Figure 1), which is not a natural product but which behaves like bilirubin in metabolism. Their lipophilicity is thought to stem from a strong tendency to fold into ridge-tile conformations that are stabilized by a web of intramolecular hydrogen bonds. Whether the folded structure is maintained at the glucuronosyl transferase catalytic site is not known, but studies of bilirubin analogues suggest that it is.^{13a,b} Glucuronidation converts the pigment to derivatives that are more polar and more water-soluble and that are excreted expeditiously in bile. The mechanisms by which bilirubin enters hepatocytes and by which the glucuronides are subsequently expelled into bile are controversial and unclear. The prevailing view is that both processes involve specific membrane-embedded transport proteins.⁷ These proteins are thought to be also involved in similar transmembrane transport of a variety of other compounds with little structural resemblance to each other or to bilirubin. If binding to transport proteins is involved, three-dimensional structure and polarity would be expected to be important determinants of hepatic uptake and biliary excretion. However, these factors have received little systematic study.

Bile from homozygous Gunn rats contains only a very low concentration of unconjugated bilirubin, even after intravenous injection of exogenous bilirubin. Although mesobiliverdin-XIII α (Figure 2) behaved like natural bilirubin when it was administered intravenously to homozygous Gunn rats, its C(10)-oxo analogue (**1**, Figure 1) did not. As shown in Figure 9c, after injection of small boluses (<1 mg/kg) of **1**, it was rapidly excreted intact in bile and was no longer detectable by HPLC in serum 2 h after injection (data not shown). In contrast, when **1** was injected into normal Sprague–Dawley rats, the intact pigment as well as two metabolites, more polar than the parent compound, appeared promptly in bile, along with bilirubin metabolites (diglucuronide and two isomeric monoglucuronides) as shown by the emergence of strong new peaks on HPLC (Figure 9a). The concentration of these new metabolites peaked at about 15 min and then slowly dwindled toward zero (Figure 9b). After ~1–2 h, **1** and its metabolites were undetectable in serum. The metabolites had broad double-humped absorption spectra that resembled those of the corresponding parent

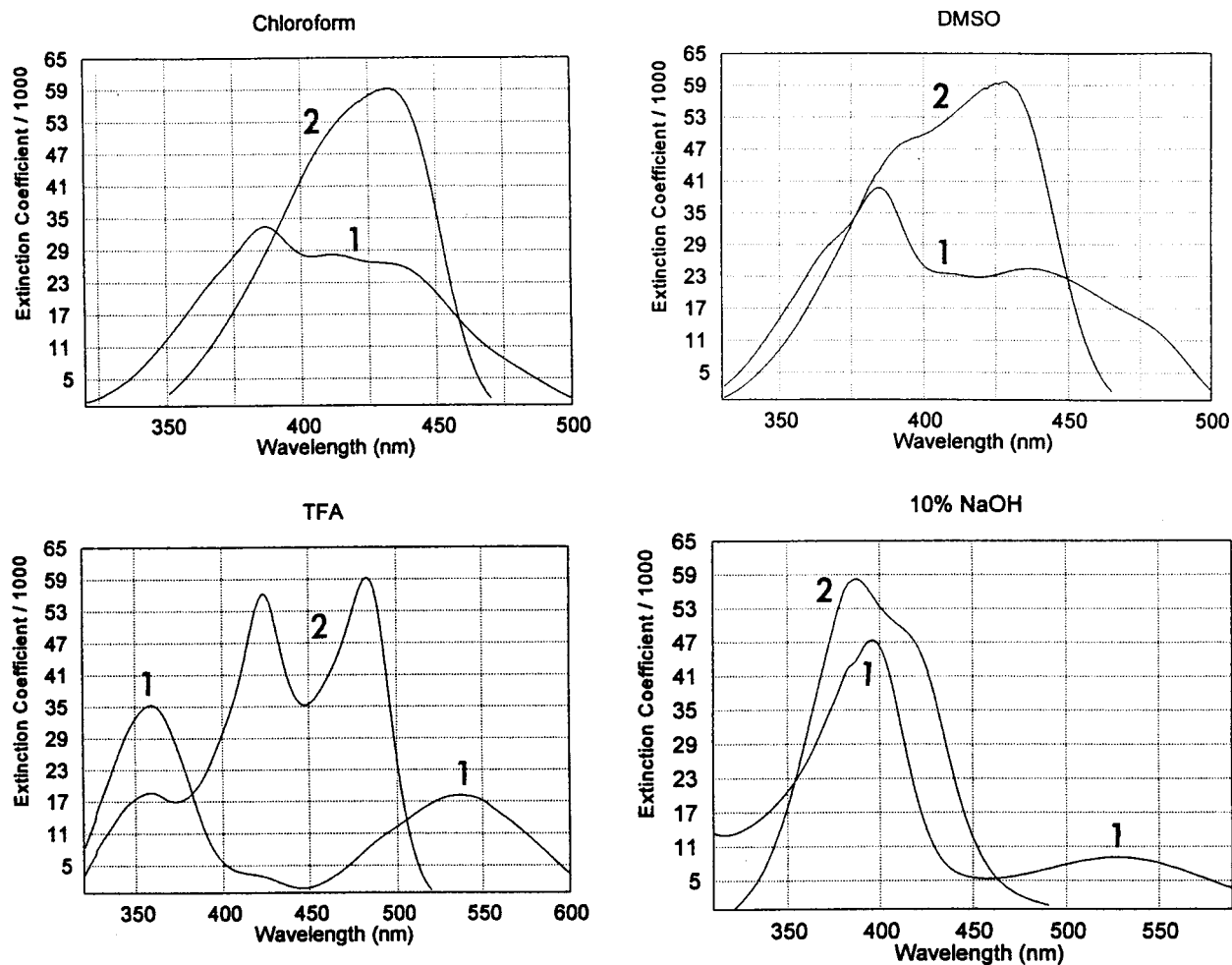


Figure 6. UV-Vis spectra of oxo-rubin **1** (spectrum 1) and mesobilirubin-XIII α (spectrum 2) in chloroform, **1**, ϵ_{389}^{\max} 33400, $\epsilon_{429}^{\text{sh}}$ 34000 and **2**, ϵ_{431}^{\max} 57800; dimethyl sulfoxide, **1**, ϵ_{383}^{\max} 40500, ϵ_{453}^{\max} 27500 and **2**, $\epsilon_{397}^{\text{sh}}$ 49100, ϵ_{426}^{\max} 57000; trifluoroacetic acid (TFA), **1**, ϵ_{356}^{\max} 35600, ϵ_{537}^{\max} 22200 and **2**, ϵ_{360}^{\max} 18600, ϵ_{423}^{\max} 56200, ϵ_{484}^{\max} 59200; 10% aqueous NaOH, **1**, ϵ_{397}^{\max} 47600, ϵ_{531}^{\max} 9900 and **2**, ϵ_{388}^{\max} 33400, $\epsilon_{417}^{\text{sh}}$ 48000.

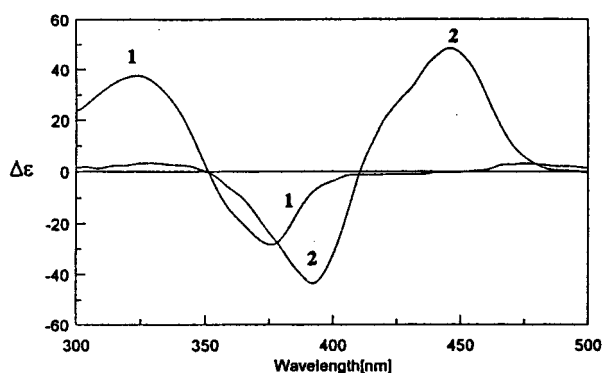


Figure 7. Circular dichroism spectra of **1** (Spectrum 1) and mesobilirubin-XIII α (Spectrum 2) at $\sim 10^{-5}$ M concentration in the presence of 10^{-3} M HSA at pH 7.8.

compound, with similar absorption maxima. On brief treatment of bile with β -glucuronidase, which is specific for β -glucuronides, or with dilute NaOH, the metabolites were converted to **1**.

Since **1** was excreted rapidly in bile in Gunn rats as well as Sprague-Dawley rats, like bilirubin and mesobilirubin it must be taken up rapidly by the liver. Therefore, the large difference in polarity within this group of compounds does not have a discriminatory effect on hepatic uptake.

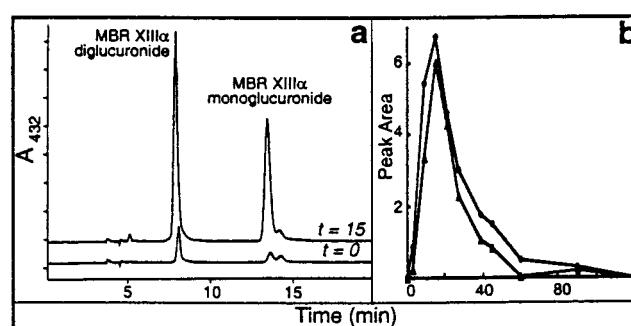


Figure 8. Metabolism of mesobilirubin-XIII α in the rat. (a) HPLC chromatograms of normal rat bile before ($t = 0$) and after ($t = 15$ min) injecting 0.25 mg of mesobilirubin-XIII α intravenously into a Sprague-Dawley rat. At $t = 0$, the chromatogram shows the presence of bilirubin diglucuronide (main peak) and its two regio-isomeric monoglucuronides. (b) Biliary excretion curves for mesobilirubin-XIII α mono and diglucuronides plotted as corrected HPLC peak area vs time postinjection of pure mesobilirubin-XIII α .

Concluding Comments

In this paper we describe the first high-yield total synthesis, and characterization, of a C(10)-oxo-rubin (**1**). The studies show that introduction of the C(10)-oxo function has a marked effect on the UV-vis and CD spectroscopic properties of the compound, making it markedly more polar (based on HPLC and TLC) than the parent C(10)-dihydro compound. The

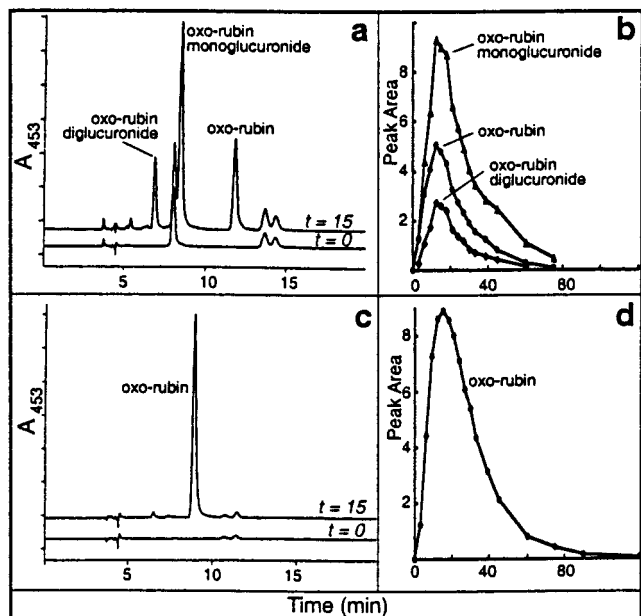


Figure 9. Metabolism and biliary excretion of C(10) oxo-rubin **1** in Sprague–Dawley and Gunn rats. (a) HPLC chromatograms of normal rat bile before ($t = 0$) and after ($t = 15$ min) intravenous injection of 0.25 mg of **1** into a Sprague–Dawley rat. At $t = 0$, the chromatogram shows the presence of bilirubin diglucuronide (main peak) and its two regio-isomeric monoglucuronides. (b) Biliary excretion profiles for **1** and its mono- and diglucuronides based on HPLC peak areas. (c) HPLC chromatograms of bile before ($t = 0$) and after ($t = 15$ min) intravenous injection of **1** (0.25 mg) into a Gunn rat. (d) Biliary excretion profile of **1** in the Gunn rat based on HPLC peak areas. Note that the chromatographic conditions for a and c were slightly different, resulting in different retention times for **1**.

energetically most stable conformation of the oxo-rubin is still the folded ridge-tile structure preferred by bilirubin and mesobilirubin-XIII α , but the presence of the C(10)-oxo group favors an increased contribution from energetically less stable non-hydrogen-bonded conformers. Surprisingly, introduction of the enolizable oxygen function at C10 does not increase the partition coefficient of the compound enough to make it extractable from CHCl₃ into aqueous NaHCO₃ solution. Nor, *in vivo*, does it prevent rapid uptake of the compound from blood into the liver or its glucuronidation by bilirubin glucuronosyl transferase. However, our experiments show that introduction of the oxo group does have a marked effect on other biological properties. In particular, it converts mesobilirubin-XIII α from a substance that requires glucuronidation for efficient excretion in bile to one that does not and, apparently, changes it from a substance that is not pumped by canalicular membrane transporters into bile to one that is. Although the C(10)-oxo-rubin does not require glucuronidation for hepatic elimination in bile, as shown by our experiments in glucuronosyl transferase-deficient Gunn rats, during its passage through the liver in normal rats there is competition between canalicular excretion in intact form and glucuronidation. Thus, both glucuronides and unchanged pigment appear promptly in bile after injection of the compound intravenously. In this respect, the C(10)-oxo-rubin **1** behaves like bilirubin monoglucuronides and rather differently from other substituted bilirubins with geminal dimethyl substitution at C10.^{13b} Taken overall, our studies show that modest chemical modification at the ridge-tile seam of bilirubin can influence the molecule's lipophilicity in a surprising manner and have a major effect on the overall metabolism and excretion of the pigment. These effects can be attributed to weakening of intramolecular hydrogen bonding in **1** and a greater contribution

from conformers that are energetically less favored for the corresponding unsubstituted analogue or for natural bilirubin.

One stimulus for undertaking these studies was the suggestion that oxidation of bilirubin at C(10) might be an alternate pathway for bilirubin metabolism and elimination. Our studies indicate that, if C(10)-oxo bilirubin was formed *in vivo*, it would undoubtedly be excreted in bile unchanged or in admixture with its glucuronides. In other studies we have found no evidence for the presence of C(10)-oxo-bilirubin in bile of Gunn rats undergoing phototherapy. Therefore, it is unlikely that oxidation at C(10) plays any role in phototherapy of neonatal jaundice.¹² Since chromatograms of Gunn rat bile from animals kept in the dark show no evidence for the presence of a C(10)-oxo-rubin, it is also unlikely that C(10) oxidation makes an important contribution to the alternate pathways of bilirubin elimination. However, if C(10) oxidation could be promoted in patients with deficient bilirubin conjugation, it would undoubtedly enhance the elimination of bilirubin and decrease the bilirubin concentration in blood.

Experimental Section

NMR spectra were obtained at 300 and 500 MHz in CDCl₃ (unless otherwise noted), and chemical shifts were reported in parts per million. UV–vis spectral data were determined in spectral grade solvents (Aldrich or Fisher). HRMS were obtained at the Midwest Center for Mass Spectrometry, University of Nebraska, Lincoln, and GC-MS analyses were carried out on a capillary gas chromatograph (30 m DB-1 column) equipped with a mass selective detector. Combustion analyses were done by Desert Analytics, Tucson, AZ. Analytical thin-layer chromatography (TLC) was carried out on J. T. Baker silica gel IB–F plates (125 μ m layer); radial chromatography was carried out on Merck silica gel PF₂₅₄ with CaSO₄, preparative layer grade. For HPLC analyses, detection was at in the range \sim 410–460 nm, depending on the pigments being analyzed, and the column was a Beckman–Altex ultrasphere-IP 5 μ m C-18 ODS column (25 \times 0.46 cm) fitted with a similarly packed precolumn (4.5 \times 0.46 cm). The flow rate was 0.75–1.0 mL/min, the elution solvent was 0.1 M di-*n*-octylamine acetate in 5–8% aqueous methanol,^{13b} and the column temperature was \sim 34 $^{\circ}$ C. Di-*n*-octylamine was obtained from Aldrich and HPLC grade MeOH from Fisher, β -glucuronidase (*E. coli* Type VII-A, 1000 units/vial), phosphatidyl choline (Type XV-E), cholesterol, taurine, sodium cholate, and human serum albumin (defatted) were obtained from Sigma. Mesobilirubin-XIII α was prepared by synthesis and by catalytic hydrogenation of bilirubin-XIII α in NH₃/MeOH.¹ Other reagents and chemicals were from Aldrich, Fisher, or Pfaltz and Bauer. Tetrahydrofuran was dried by distillation from LiAlH₄; methanol was distilled from Mg(OCH₃)₂; and dimethyl sulfoxide was freshly distilled from CaH₂ under vacuum. Melting points are uncorrected. Homozygous male Gunn rats, weighing 300–400 g, were obtained from our own colony, and Sprague–Dawley male rats, weight 370–520 g, were obtained from local commercial vendors. *In vivo* studies were done in a windowless room under safe lights.

5,5'-Bis(*tert*-butoxycarbonyl)-4,4'-dimethyl-3,3'-bis(methoxycarbonyl)ethyl-2,2'-dipyrrylmethane (5). 5-Acetoxyethyl-4-methyl-3-methoxycarbonyl-2-(*t*-butoxycarbonyl)-pyrrole **6**^{30–32} (10.0 g, 29 mmol) was dissolved in aqueous acetic acid (80%, 180 mL). The solution was stirred while *p*-toluenesulfonic acid monohydrate (500 mg) was added and then allowed to stir at room temperature for 7 h. Dichloromethane (300 mL) and water (300 mL) were added, and the organic layer was separated. The aqueous layer was extracted with dichloromethane (2 \times 100 mL), and the combined organic phases were washed successively with 10% ammonia (100 mL), water (2 \times 200 mL), and brine (200 mL). After drying over anhydrous sodium sulfate,

(30) Lightner, D. A.; McDonagh, A. F. *Acc. Chem. Res.* **1984**, *17*, 417–24.

(31) Smith, K. M.; Pandey, R. K. *J. Heterocycl. Chem.* **1983**, *20*, 1383–1388.

(32) Johnson, A. W.; Kay, I. T.; Markham, E.; Price, R.; Shaw, K. B. *J. Chem. Soc.* **1959**, 3416–3424.

the solvent was removed under reduced pressure, and the residue was crystallized from dichloromethane-hexane to yield **5**, 7.05 g (87%) yield: mp 137–139 °C (lit. 127 °C,³³ 132–134 °C³⁴). ¹H NMR (300 MHz): δ 1.54 (s, 18H), 2.23 (s, 6H), 2.47 (t, $J = 7.32$ Hz, 4H), 2.74 (t, $J = 7.32$ Hz, 4H), 3.93 (s, 6H), 8.69 (s, 2H), ppm. ¹³C NMR (75 MHz): δ : 10.38 (pyrr-CH₃), 19.15, 22.43, 28.30, 34.51, 51.46, 80.12, 119.50, 119.83, 125.39, 129.05, 160.94, 173.46 ppm.

5,5'-Diformyl-4,4'-dimethyl-3,3'-bis(methoxycarbonyl)-2,2'-dipyrrylmethane (4). Finely ground 5,5'-bis(*tert*-butoxycarbonyl)-4,4'-dimethyl-3,3'-bis(methoxycarbonyl)-2,2'-dipyrryl-methane (**5**) (0.64 g, 1.17 mmol) was added in portions (100 mg) to cooled (~0 °C) trifluoroacetic acid (3 mL) with stirring. Effervescence was observed. After bubbling ceased, trimethyl orthoformate (0.6 mL, 0.58 g, 5.5 mmol, 4.7 molar equiv) was added at once. The mixture was stirred for another 5 min at 0° before pouring into water (50 mL). The product was precipitated as pink solid using dilute ammonia (10%) to adjust the pH to 8. The solid was collected by suction filtration, washed with water (5 × 50 mL), and dried before recrystallizing from dichloromethane-hexane to yield **4** (0.38 g, 80%): mp 179–180 °C (lit.³³ 179–181 °C). IR (KBr, film) ν : 3412, 3236, 2931, 1731, 1619, 1508, 1443, 1378, 1303, 1249, 1167, 1061, 961, 737, 607 cm⁻¹. ¹H NMR (300 MHz): δ : 2.29 (s, 6H), 2.53 (t, $J = 6.80$ Hz, 4H), 2.80 (t, $J = 6.80$ Hz, 4H), 3.71 (s, 6H), 4.05 (s, 2H), 9.46 (s, 2H), 10.21 (s, 2H) ppm. ¹³C NMR (75 MHz): δ : 8.70, 18.86, 22.38, 34.04, 51.70, 120.91, 128.85, 134.71, 173.47, 176.48 ppm.

5,5'-Diformyl-4,4'-dimethyl-3,3'-bis(methoxycarbonyl)-2,2'-dipyrryl ketone (3). 5,5'-Diformyl-4,4'-dimethyl-3,3'-bis(methoxycarbonyl)-2,2'-dipyrrylmethane (**4**) (1.79 g, 4.4 mmol) was dissolved in acetic acid (40 mL) by heating on a water bath to 40 °C. After removing the water bath, a solution of ceric (IV) ammonium nitrate (CAN, 14.6 g, 26.7 mmol, 6 molar equiv) in acetic acid (20 mL) and water (20 mL) (CAN was first dissolved in water, then diluted with acetic acid) was added dropwise over 10 min at room temperature. The color of the solution turned from dark brown to red, then light red, yellow, and finally to an orange color. The mixture was allowed to stir for an additional 20 min at room temperature before pouring into ice-water (~200 mL). After extraction with dichloromethane (3 × 100 mL), the combined extracts were washed successively with water (2 × 50 mL), 5% aqueous sodium bicarbonate (50 mL), and brine (50 mL). The solution was dried over anhydrous sodium sulfate and concentrated (rotovap). The residue was crystallized from 80% methanol-water to give the desired product **3**, (963 mg, 52%): mp 206–208 °C (lit.³³ 207–208 °C). IR (KBr, film) ν : 3213, 3001, 2931, 2860, 1731, 1637, 1543, 1461, 1372, 1290, 1237, 1172, 1073, 897, 861, 826, 726, 609 cm⁻¹. ¹H NMR (300 MHz): δ 2.41 (s, 6H), 2.67 (t, $J = 7.32$ Hz, 4H), 3.63 (s, 6H), 9.12 (s, 2H), 11.31 (s, 2H) ppm. ¹³C NMR (75 MHz): δ 8.05, 18.82, 33.96, 51.23, 129.79, 130.60, 130.83, 133.77, 173.15, 178.18 ppm.

2-Tosyl-3-ethyl-4-methylpyrrole (8). This compound appears in the literature³⁵ with no experimental details or spectroscopic properties. 2-Nitro-3-pentanol was prepared according to a literature procedure³⁶ and acetylated to give 2-nitro-3-acetoxy-pentane. To a mixture of tosylmethyl isocyanide (TosMIC, 46 g, 0.24 mol, 1.0 molar equiv) and 1,1,3,3-tetramethylguanidine (63 mL, 58 g, 0.5 mol, 2.1 molar equiv), a solution of 2-nitro-3-acetoxypropane (42 g, 0.24 mol) in dry THF (100 mL) and 2-propanol (100 mL) was added dropwise over 1 h. The mixture was allowed to stir at room temperature for 70 h before removing all solvent (rotovap). The resulting dark-brown oil was taken up in 80% aqueous methanol, and the desired product (**8**) (35 g, 55% yield) was obtained after chilling at -20 °C for several hours: mp 114–116 °C. IR (KBr, film) ν : 3307, 2960, 2916, 2872, 1443, 1296, 1213, 1184, 1137, 1084, 808, 708, 661, 585 cm⁻¹. ¹H NMR (300 MHz): δ : 0.98 (t, $J = 7.32$ Hz, 3H), 1.96 (s, 3H), 2.38 (s, 3H), 2.63 (q, $J =$

7.32 Hz, 2H), 6.69 (s, 1H), 7.26 (d, $J = 7.82$ Hz, 2H), 7.77 (d, $J = 7.82$ Hz), 9.25 (s, 1H, NH) ppm. ¹³C NMR (75 MHz): δ : 9.60, 14.38, 17.27, 21.28, 120.47, 120.91, 122.92, 126.41, 129.50, 130.79, 140.16, 143.25 ppm.

An Improved Synthesis of *p*-Toluenesulfonylisocyanide (TosMIC). In a one liter round-bottom flask, equipped with a mechanical stirrer and a reflux condenser, were placed sodium *p*-toluenesulfonate hydrate (80 g, 97%, 0.43 mol), paraformaldehyde (39 g, 1.31 mol, 3.0 molar equiv), formamide (69 mL, 1.76 mol, 4.0 molar equiv), and formic acid (99%, 83 mL, 2.18 mol, 5.0 molar equiv). The mixture was heated slowly to 90 °C and stirred for 2 h at the same temperature before being poured into ice-salt (500 g of ice and 50 g of salt). After 2 h, the white crystalline product was collected by suction filtration, washed with cold water (2 × 30 mL), and dried in a desiccator over phosphorus pentoxide under vacuum to yield *N*-(*p*-toluenesulfonylmethyl)formamide (84 g, 90%), which was sufficiently pure for the next step. It had mp 104–107 °C (lit.¹⁹ 106–110 °C). ¹H NMR (300 MHz): δ : 2.34 (s, 3H, CH₃), 4.69 (d, $J = 6.83$ Hz, 2H, CH₂), 6.85 (brs, 1H, NH), 7.34 (d, $J = 8.3$ Hz, 2H, 2,6-Ar-H), 7.80 (d, $J = 8.3$ Hz, 2H, 3,5-Ar-H), 8.07 (s, 1H, CHO) ppm. ¹³C NMR (75 MHz): δ : 21.49 (CH₃), 58.79 (CH₂), 128.69 (2,6-Ar), 129.89 (3,5-Ar), 133.67 (1-Ar), 145.51 (4-Ar), 160.39 (CHO) ppm.

A three-neck round-bottom flask, equipped with a mechanical stirrer, reflux condenser, drying tube containing anhydrous calcium chloride, thermometer, and 100 mL dropping funnel was charged with *N*-*p*-toluenesulfonylmethylformamide (69 g, 0.32 mol), dry tetrahydrofuran (150 mL), anhydrous ether (60 mL), and triethylamine (140 mL). The stirred suspension was chilled to -5 °C using an ice-salt bath. Then a solution of phosphorus oxychloride (53 g, 0.35 mol, 1.07 molar equiv) in dry tetrahydrofuran (40 mL) was added dropwise from the dropping funnel at a rate such that the temperature was maintained between -5 °C and 0 °C. During the reaction, the *N*-(*p*-tolyl-sulfonylmethyl)-formamide gradually dissolved and triethylamine salts precipitated. Near the completion of the reaction the white suspension slowly turned brown. After being stirred for another 30 min at 0 °C, the mixture was poured into two liters of ice-water with continuous stirring. The solid material dissolved to give a clear, dark-brown solution before the product began to separate as a fine, brown crystalline solid. The mixture was stirred for 30 min at 0 °C, and the precipitate was collected by suction filtration and washed with cold water (100 mL). After drying in air, TosMIC was obtained (60 g, 95%) that is pure enough for synthetic purposes. It had mp 112–114 °C (lit.¹⁹ 111–114 °C). ¹H NMR (300 MHz): δ : 2.50 (s, 3H, CH₃), 4.58 (s, 2H, CH₂), 7.46 (d, $J = 7.84$ Hz, 2H, 2,6-Ar), 7.91 (d, $J = 7.84$ Hz, 2H, 3,5-Ar) ppm. ¹³C NMR (75 MHz): δ : 21.59 (CH₃), 60.91 (CH₂), 129.24 (2,6-Ar), 130.16 (3,5-Ar), 131.96 (1-Ar), 146.68 (4-Ar), 166.08 (N=C) ppm.

5-Bromo-4-methyl-3-ethyl-2-tosyl-pyrrole (9). 2-Tosyl-2-ethyl-4-methylpyrrole (**8**) (13.35 g, 0.05 mol) was dissolved in dichloromethane (150 mL) and chilled to -5 °C using an ice-salt bath. Then, a solution of bromine (8.12 g, 0.05 mol, 1.0 molar equiv) in dichloromethane (100 mL) was added dropwise over 20 min. After the addition was complete, the reaction was allowed to stir for a further 10 min at the same temperature. Dilute aqueous ammonia (10%, 200 mL) was added dropwise to neutralize the acid; the organic layer was separated; and the aqueous layer was extracted with dichloromethane (3 × 100 mL). The combined organic phases were washed with saturated sodium bicarbonate (2 × 100 mL), water (100 mL), and brine (100 mL). After drying over anhydrous sodium sulfate, the solvent was evaporated, and the crude brown product was crystallized from dichloromethane-hexane to yield a white product (**9**) (16.5 g, 95% yield): 162–164 °C (lit.³⁷ 163–164 °C). IR (KBr, film) ν : 3260, 2970, 2931, 2884, 1596, 1490, 1367, 1302, 1202, 1167, 1137, 1102, 808, 714, 579 cm⁻¹. ¹H NMR (300 MHz): δ : 0.97 (t, $J = 7.32$ Hz, 3H), 2.30 (s, 3H), 2.40 (s, 3H), 2.46 (q, $J = 7.32$ Hz, 2H), 7.24 (d, $J = 7.80$ Hz, 2H), 7.79 (d, $J = 7.80$ Hz, 2H), 9.16 (s, 1H, NH) ppm. ¹³C NMR (75 MHz): δ : 9.23, 14.97, 21.40, 21.66, 106.19, 121.20, 122.30, 129.10, 131.01, 139.45, 142.64, 145.20 ppm. GC-MS *m/z* (%): 343 [M⁺ + 1] (93), 342 [M⁺] (100), 278 (8), 263 (7), 204 (29), 188 (20), 140 (44), 106 (60), 65 (63) amu.

(33) Clezy, P. S.; Fookes, C. J. R.; Liepa, A. J. *Austral. J. Chem.* **1972**, *25*, 1979–1990.

(34) Ono, N.; Kawamura, H.; Bougauchi, M.; Maruyama, K. *Tetrahedron* **1990**, *46*, 7483–7496.

(35) Kohori, K.; Kimoshita, H.; Inomata, K. *Chem. Lett.* **1995**, 799–800.

(36) Kambe, S.; Yasuda, H. *Bull. Chem. Soc. Jpn.* **1968**, *41*, 1444–1446.

(37) Kinoshita, H.; Hayashi, Y.; Murata, Y.; Inomata, K. *Chem. Lett.* **1993**, 1437–1440.

5-Tosyl-4-ethyl-3-methyl-pyrrolin-2-one (10). 2-Tosyl-3-ethyl-4-methyl-5-bromopyrrole (**9**) (2.0 g, 5.8 mmol) was dissolved with stirring in trifluoroacetic acid (25 mL). Then, water (5 mL) was added dropwise over 2 min. After being stirred at room temperature for 4 h, the solution was taken up into dichloromethane (100 mL). Water (100 mL) was added, and the organic layer was separated. The aqueous layer was extracted with dichloromethane (3 × 50 mL), and the combined organic phases were washed with sodium bicarbonate (2 × 100 mL), water (100 mL), and brine (100 mL). After drying over anhydrous sodium sulfate, the solvent was removed and the crude brown product was crystallized from dichloromethane–hexane to yield **10** (1.38 g, 85% yield): mp 165–167 °C (lit.³⁸ 154–155 °C). IR (KBr, film): 3189, 3072, 2960, 2931, 2860, 1702, 1595, 1449, 1390, 1307, 1208, 1143, 1078, 814, 667, 597, 556 cm⁻¹. ¹H NMR (300 MHz) δ: 1.19 (t, *J* = 7.32 Hz, 3H), 1.57 (s, 3H), 2.41 (s, 3H), 2.56, 2.62 (m, 2H), 5.16 (s, 1H), 7.00 (s, 1H, NH), 7.27 (d, *J* = 7.84 Hz, 2H), 7.63 (d, *J* = 7.84 Hz, 2H) ppm. ¹³C NMR (75 MHz) δ: 8.16, 12.77, 20.13, 21.49, 76.68, 129.24, 129.48, 130.28, 130.44, 145.69, 148.62, 173.17 (C=O) ppm. GC-MS *m/z* (%): 279 [M⁺] (8), 198 (2.8), 155 (24), 139 (100), 123 (31), 91 (56) amu.

3-Methyl-4-ethylpyrrolin-2-one (3). 1-Tosyl-3-ethyl-4-methylpyrrolin-2-one (**10**) (1.57 g, 5.6 mmol) was added to ethanol (50 mL), and the mixture was slowly warmed using a water bath, all while stirring continuously. After all of the solid material had dissolved, sodium borohydride (0.21 g, 5.6 mmol, 1.0 molar equiv) was added in small portions over 5 min. The reaction was allowed to stir an additional 20 min before more sodium borohydride (0.21 g, 5.6 mmol, 1.0 molar equiv) was added. After another 20 min of stirring, the solvent was removed (rotovap), and the resulting brown residue was evacuated for 4 h at ~1 mm Hg. It was then taken up into dichloromethane (100 mL), and inorganic solids were removed by filtration. The residue was washed with dichloromethane (3 × 30 mL), and the combined organic solutions were passed through a short column of anhydrous sodium bicarbonate. Evaporation of the solvent (rotovap) yielded the desired product as a white solid (0.63 g, 90%): mp 78–80 °C (lit.³⁸ 77–78 °C). IR (KBr, film): 3236, 2960, 1596, 1514, 1484, 1449, 1313, 1155, 1084, 808, 726, 691, 661, 573 cm⁻¹. ¹H NMR (300 MHz) δ: 1.09 (t, *J* = 7.32 Hz, 3H), 1.78 (s, 3H), 2.40 (q, *J* = 7.32 Hz), 2H, 3.82 (s, 2H), 7.17 (brs, 1H, NH) ppm. ¹³C NMR (75 MHz) δ: 7.95, 12.37, 20.91, 47.66, 127.53, 154.26, 176.16 ppm. GC-MS *m/z* (%): 125 [M⁺] (17), 110 (35), 82 (36), 96 (100), 68 (28), 53 (26) amu.

3,17-Diethyl-1,10,19,21,23,24-hexahydro-2,7,13,18-tetramethyl-1,10,19-trioxo-21H-bilin-8,12-dipropanoic acid (10-oxo-mesobilirubin-XIII α) (1). A mixed suspension of 5,5'-diformyl-4,4'-dimethyl-3,3'-bismethoxyethyl-2,2'-dipyrryl-ketone (**2**) (100 mg, 0.24 mmol), 3-methyl-4-ethyl-2-pyrrolinone (**3**) (300 mg, 2.4 mmol, 10 molar equiv), potassium hydroxide (5 g, 89 mmol), methanol (40 mL), and water (10 mL) was heated at reflux for 50 h with continuously stirring. The mixture was cooled to 0 °C, diluted with cold water (200 mL), and extracted with dichloromethane (6 × 60 mL). (The aqueous phase (**A**) was used for isolating the product as in the next paragraph.) The combined organic extracts were washed successively with water (2 × 50 mL), aqueous sodium bicarbonate (50 mL), and brine (50 mL). After drying over anhydrous sodium sulfate, the solvent was removed (rotovap) to yield unreacted 3-methyl-4-ethyl-2-pyrrolinone (40 mg, 16% recovered).

To the aqueous phase (**A**) from above was carefully added concentrated hydrochloric acid (30%) to pH 2 to precipitate a red solid, which was collected by centrifugation. The solid was slurried with water and collected again by centrifugation. This procedure was repeated three times to remove any water-soluble impurities, and the crude red product was finally collected by suction filtration. After air-drying, the crude product weighed 136 mg (94% yield) and was estimated to be >90% pure, as judged by ¹H NMR in (CD₃)₂SO. It could be purified further by dissolving in a minimum amount of dry pyridine (dried over

potassium hydroxide) followed by addition of methanol (5 mL), then anhydrous ether to effect precipitation. The precipitate was collected by suction filtration and dissolved in a minimum amount of dry pyridine again to repeat the precipitation process. Pure product was finally obtained as reddish fluffy solid by repeating this procedure 3 or 4 times to afford **1** (112 mg, 77% yield): mp 238–240 °C (dec). IR (KBr, film) ν : 3331, 2978, 2931, 1678, 1490, 1443, 1384, 1273, 1161, 978, 761, 673 cm⁻¹. ¹H NMR (DMSO-*d*₆, 300 MHz) δ: 1.07 (t, *J* = 7.32 Hz, 6H), 1.75 (s, 6H), 2.07 (s, 6H), 2.31 (t, *J* = 7.32 Hz, 4H), 2.52 (q, *J* = 7.32 Hz, 4H), 2.69 (t, *J* = 7.32 Hz, 4H), 5.97 (s, 2H), 10.20 (s, 2H), 10.89 (s, 2H), 12.00 (s, 2H) ppm. ¹H NMR (pyridine-*d*₅, 300 MHz) δ: 1.08 (t, *J* = 7.32 Hz, 6H), 1.88 (s, 6H), 2.12 (s, 6H), 2.46 (q, *J* = 7.32 Hz, 4H), 3.01 (t, *J* = 7.32 Hz, 4H), 3.40 (t, *J* = 7.32 Hz, 4H), 6.22 (s, 2H), 10.80 (s, 2H), 12.00 (s, 2H) ppm. (The COOH peak was not observed because of formation of the pyridine salt.) ¹³C NMR (DMSO-*d*₆, 75 MHz) δ: 8.39, 9.39, 14.84, 17.46, 20.49, 35.03, 96.40, 122.92, 125.97, 128.22, 129.16, 131.55, 133.61, 147.68, 172.83, 174.09, 176.01 ppm. FAB-HRMS: calcd for C₃₃H₃₈N₄O₇, 602.2740; found, 602.2737.

Animal Studies. The experimental procedures used for studying the hepatic metabolism and biliary excretion of oxo-rubin **1** and mesobilirubin-XIII α in Gunn and normal rats are described in detail elsewhere.^{1,13b} Briefly, a femoral vein and the common bile duct were cannulated, and a liposomal solution^{13b} containing phosphatidyl choline (1.5 g), cholesterol (62 mg), sodium cholate (12.95 g), and taurine (3.75 g) in 1 L of water was infused (2 mL/h) through the femoral catheter to maintain hydration of the animal and to ensure a steady bile flow rate (measured gravimetrically). After the bile flow rate and body temperature had stabilized (~30–60 min), oxo-rubin or mesobilirubin-XIII α (0.25 mg), dissolved in rat serum (1 mL) with the aid of a small volume (0.1 mL) of DMSO, was infused via the femoral vein as a bolus over a period of about one minute. Bile was collected in 20 μ L aliquots from the tip of the bile duct cannula immediately before injection of pigment and at frequent intervals thereafter over a period of 4 h. Collection of each sample took about 20 s. Immediately after collection, bile samples were flash frozen in dry ice and then kept at -70 °C in the dark until analyzed by HPLC. Blood samples were collected from a small incision in the tip of the tail and allowed to clot, and serum collected by centrifugation was frozen and stored as for bile. For HPLC, bile and serum samples (20 μ L) were mixed with 80 μ L of ice-cold 0.1 M methanolic di-*n*-octylamine acetate (prepared by dissolving equimolar quantities of di-*n*-octylamine and acetic acid in methanol) and microfuged for 30 s, and 20 μ L of the clear supernate was injected onto the column. Biliary excretion curves were derived by plotting HPLC peak areas, determined by integration, against time and are not corrected for small variations in bile flow rate. For hydrolysis of glucuronides with β -glucuronidase, bile (20 μ L) was mixed with 40 μ L of β -glucuronidase solution (prepared by adding 1 mL of water to one vial of bacterial β -glucuronidase on ice), and the mixture was incubated for 1 h at 37 °C in the dark and then mixed vigorously with 140 μ L of 0.1 M di-*n*-octylamine acetate in methanol. This mixture was microfuged for 30–60 s, and an aliquot (20 μ L) of the supernate was taken for HPLC. For base hydrolysis of glucuronides, bile (20 μ L) was mixed with 1 M NaOH (10 μ L). After 3 min at room temperature, 10 μ L of 1 M HCl was added, followed, after mixing, by 160 μ L of 0.1 M di-*n*-octylamine acetate in methanol. The mixture was vortexed and microfuged for 30–60 s, and an aliquot (20 μ L) of the supernate was taken for HPLC.

Acknowledgment. We thank the National Institutes of Health (HD-17779, DK26307, and GM36633) for support of this research.

JA991814M